

Towards ultimate fragmentation functions at future lepton colliders

Bin Zhou^{a,b} and Jun Gao^{a,b}

^a*INPAC, Shanghai Key Laboratory for Particle Physics and Cosmology, School of Physics and Astronomy, Shanghai Jiao Tong University, Shanghai 200240, China*

^b*Key Laboratory for Particle Astrophysics and Cosmology, Shanghai 200240, China*

E-mail: zb0429@sjtu.edu.cn, jung49@sjtu.edu.cn

ABSTRACT: In this work, we study the constraining power of future lepton colliders on fragmentation functions (FFs) to light charged hadrons from quarks and gluon in the framework of QCD collinear factorization. We perform analyses of FFs by including a wide range of pseudo-data from future lepton colliders, such as measurements on hadron multiplicities in the inclusive production of two jets and W boson pairs, at various center of mass energies, and from hadronic decays of the Higgs boson, including both to heavy quarks and to gluons. The high luminosity and high energies of future lepton colliders allow for quark flavor separations and ensure a precise determination of FFs based solely on data from electron-positron collisions. We find that either CEPC, FCC- ee or ILC can significantly reduce the uncertainties of FFs in a wide kinematic range, compared to the NPC23 set obtained with a global analyses to current world data. We also discuss the impact of higher-order QCD corrections, and the potential constraints from measurements of three-jet production. Furthermore, we describe an update of the FMNLO program allowing for calculating hadron production cross sections at next-to-next-to-leading order in QCD, which is used in this study.

Contents

| | | |
|----------|---|-----------|
| 1 | Introduction | 2 |
| 2 | Pseudo-data generation | 3 |
| 2.1 | FFs-sensitive processes | 3 |
| 2.2 | Theory calculations and pseudo-data generation | 5 |
| 2.3 | Theoretical setup and fit of FFs | 8 |
| 3 | Results and discussions | 11 |
| 3.1 | The constraints to FFs from future lepton colliders | 11 |
| 3.2 | Alternative fit | 13 |
| 3.3 | The constraints from three-jet production | 19 |
| 4 | Summary | 21 |
| A | NNLO calculations in FMNLO | 22 |
| B | Three-jet production in FMNLO | 23 |

1 Introduction

A comprehensive grasp of the hadronization of quarks and gluons into hadrons is a fundamental element of theoretical predictions for specific high-energy processes with identified hadrons, including single-inclusive hadron production in electron-positron annihilation (SIA), semi-inclusive deep inelastic lepton-nucleon scattering (SIDIS) and single-inclusive hadron production in proton-proton (pp) collisions. This is quantified by fragmentation functions (FFs), which, in the simplest picture, describe the probability distribution on the fraction of the initial parton momentum carried by the identified hadron [1–3].

As the FFs are related to a nonperturbative aspect of QCD, they cannot be calculated with precision using theoretical methods and in general extracted from fits to a variety of experimental data. Many studies have already been conducted on a comprehensive fit involving various data samples to extract FFs. The most notable contributions in this field can be found in the works of DSS [4], AKK [5], NNFF [6], MAPFF [7], JAM [8], and NPC23 [9, 10], which combine data sets from SIA, SIDIS, or pp collisions. In contrast, the HKNS analysis only includes SIA data [11]. The aforementioned analyses are carried out at next-to-leading order (NLO) in perturbative QCD. Furthermore, determinations of FFs at next-to-next-to-leading order (NNLO) with SIA data only [12–15] and at approximate NNLO with SIA and SIDIS data [16, 17] have also been made.

In the present study, we focus on the fit based solely on the data from the lepton collider. There are numerous publicly available SIA measurements from various experiments and with different center of mass energies, including TASSO, TPC measurements below the Z -pole [18, 19], OPAL, ALEPH, DELPHI, and SLD at Z -pole [20–23], and OPAL and DELPHI above the Z -pole [24, 25]. They measured the production of π^\pm , K^\pm and p/\bar{p} separately. It is widely acknowledged that these measurements from SIA are not sensitive to the separation between quark and anti-quark FFs. Furthermore, the gluon FF is poorly constrained by SIA measurements. Consequently, a significant number of pertinent studies in the determination of light charged hadron FFs typically incorporate data from SIDIS and pp collisions to enhance the differentiation between distinct quark and antiquark flavors. However, this is beyond the scope of the present work.

With the construction and operation of future lepton colliders, such as the International Linear Collider (ILC) [26–28], the Circular Electron Position Collider (CEPC) [29–31] and the Future Circular Collider (FCC- ee) [32–34], it is also possible to give well-constrained FFs based solely on comprehensive data sets from future lepton colliders [35, 36]. In comparison to previous lepton colliders, these colliders can operate at higher collider energies and measure a greater number of observables. The CEPC and FCC- ee operate primarily at energies of 91 GeV, 160 GeV, 240 GeV and 360 GeV to perform precision measurements of the properties of the Higgs bo-

son, W and Z bosons, while the ILC runs initially at 500 GeV, then at 350 GeV and 250 GeV. The running scenarios at a wide range of center-of-mass energy will provide a substantial quantity of experimental data, which can be employed to constrain the FFs. For instance, the data from the decay of the Higgs boson to gluon can be used to constrain the FFs from gluon. Furthermore, the considerable statistical data set that a future lepton collider will generate will lead to a reduction in the statistical and systematic uncertainties.

In this study, we assess the constraining power of measurements from future lepton colliders on the FFs to light charged hadrons from quarks and gluon. We first generate pseudo-data for a number of FFs-sensitive processes at future lepton colliders. Subsequently, we utilize the NPC23 set obtained with a global analyses to current world data as an example to quantify the constraints of pseudo-data on the FFs using the fit of FFs. We then conduct various alternative fits to assess the impact of individual data sets and the effect of theoretical uncertainties on the extracted FFs. Finally, we discuss the impact of three-jet production at electron-positron colliders on the determination of FFs.

This paper is organized as follows. In Section 2 we describe the features of the various processes used to generate the pseudo-data. In Section 3 we quantify the constraints to the FFs from these pseudo-data using the fit of FFs. The summary comes in Section 4. We briefly introduce how to conduct NNLO calculations for SIA and SIDIS, as well as NLO calculations for hadron multiplicities in three jets production in the appendix, as implemented in FMNLO [37] and used in this study.

2 Pseudo-data generation

In this section, we present the various processes at future lepton colliders for which pseudo-data have been generated. Details are provided about the binning and kinematic cuts. Additionally, the baseline measurement from SLD at Z -pole [23] is described, which is used to model the experimental systematic uncertainties expected in future lepton colliders.

2.1 FFs-sensitive processes

This study begins with an examination of the diverse processes at lepton colliders that will be employed in the generation of pseudo-data. The corresponding parton-level cross sections include inclusive $q\bar{q}$ production with q representing all quark flavors except for the top quark at various center-of-mass energies, W^-W^{+*} production at the reaction threshold $\sqrt{s} \sim 2m_W$, and the three main Higgs boson decay channels. Furthermore, our analysis encompasses the heavy-flavor (either the charm or bottom quark) tagged measurements in electron-positron annihilation. The heavy-flavor tagged measurements provide crucial inputs for the determination of fragmentation functions from heavy quarks, as will be demonstrated in subsequent

sections. The specific processes for which the pseudo-data have been generated are as follows:

For Higgs boson decay processes, we generate pseudo-data for differential distribution in the energy fraction $x_h = 2E_h/\sqrt{s}$ carried by π^\pm , K^\pm and p/\bar{p} respectively. Future lepton colliders, which are designed to act as a Higgs factory, will produce and record a vast number of Higgs bosons. We choose the Higgs boson events produced at a center-of-mass energy of 240 or 250 GeV. It is known that the branching ratios of the Higgs boson decaying into bottom quark-antiquark pairs, charm quark-antiquark pairs, and gluons are 57.7%, 2.91% and 8.57%, respectively [38, 39]. Consequently, the expected number of events for the three main decay modes can be readily derived, which can then be employed to calculate the relative statistical error.

For the inclusive $q\bar{q}$ production at various center-of-mass energies, we focus on the distribution of the energy fraction carried by the identified hadron π^+ , π^- , K^+ , K^- , p and \bar{p} separately. The angle of emission of the identified charge hadrons with respect to the electron beam direction in the center-of-mass frame is required to satisfy $\cos(\theta) > 0$. These measurements are of great utility in the differentiation between the various light quarks (u , d and s quark) and antiquark flavors. Figure 1 illustrates the leading order (LO) cross section for the production of various light quarks and anti-quarks at different processes, with the total contributions for each process normalized to 1. It can be observed that the contribution from the quark and the corresponding anti-quark is significantly different at different collider energies, which is useful for the separation of light quarks and their anti-quark FFs. Furthermore, it can be observed that the contribution from the up-quark and the corresponding down-quark is markedly different at $\sqrt{s} = 91$ GeV and 160 GeV, with the contribution of the diverse quark remaining relatively unchanged as \sqrt{s} increases. The aforementioned two points ensure well-constrained FFs for light quarks. Additionally, measurements of heavy flavors tagged with the identification of the produced hadrons (π^\pm , K^\pm and p/\bar{p}) were considered, as these provide further inputs for the determination of FFs from heavy quarks. In contrast to the inclusive $q\bar{q}$ production processes, no $\cos(\theta)$ cuts are applied.

In considering the production of W^-W^{+*} at the reaction threshold $\sqrt{s} \sim 2m_W$, two cases are distinguished: inclusive hadronic and c -tagged measurements. Pseudo-data are generated for the distribution of the energy fraction carried by π^+ , π^- , K^+ , K^- , p and \bar{p} , respectively. It is important to note that the measurement of particle momentum spectra can be performed in the virtual W^* boson rest frame. Consequently, the energy fraction is defined as $2E_h/E_W^*$, where E_W^* is the energy of the virtual W^* boson in the rest frame.

It should be noted that the list of processes considered in this work is by no means exhaustive. It is evident that further significant processes will provide valuable insights into the FFs to light charged hadrons in the forthcoming lepton collider era. For instance, the impact of three-jet production on the FFs will be presented in

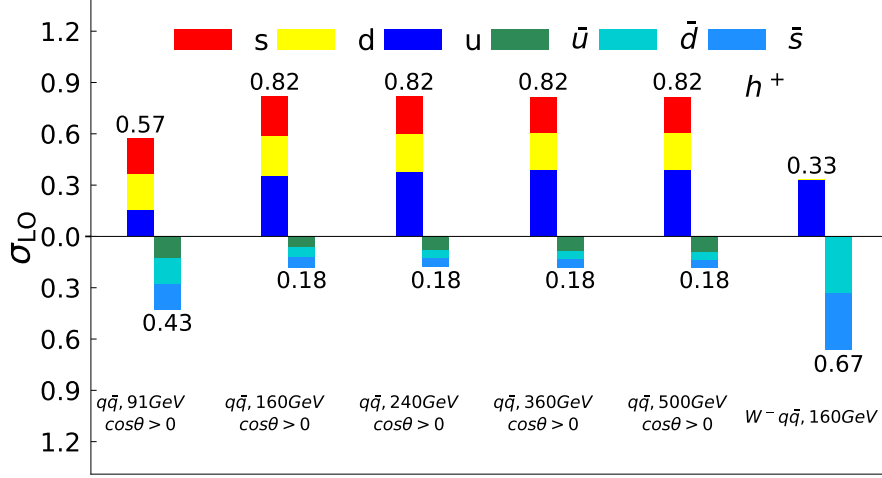


Figure 1. LO cross section for various light quarks and antiquarks production at various processes. The total contributions for each process are normalized to 1.

Section 3. Nevertheless, the set of processes considered in this work provides a sufficient snapshot of the constraining potential of future lepton colliders.

2.2 Theory calculations and pseudo–data generation

In this subsection, we will first review the factorization theorem of the cross section and fragmentation structure functions, such as in the SIA process. The SIA differential cross section at a given center-of-mass energy of $\sqrt{s} = Q$ is written as [40, 41]

$$\frac{d^2\sigma^h}{dx_h d\cos(\theta)} = \frac{3}{8}(1 + \cos^2(\theta)) F_T^h(x_h, Q^2) + \frac{3}{4}\sin^2(\theta) F_L^h(x_h, Q^2) + \frac{3}{4}\cos(\theta) F_A^h(x_h, Q^2). \quad (2.1)$$

where $F_T^h(x_h, Q^2)$, $F_L^h(x_h, Q^2)$ and $F_A^h(x_h, Q^2)$ are the transverse, longitudinal and asymmetric structure functions, respectively. These can be expressed in a factorized form of fragmentation functions $D_i^h(x_h, \mu_F^2)$ with $i = q, \bar{q}, g$ and calculable coefficient functions $C_{k,l}^{\text{S,NS}}(x_h, \mu_F^2)$ as follows [1]:

$$\begin{aligned} F_k^h(x_h, Q^2) &= \sigma_{\text{tot}}^{(0)}(Q^2) [D_S^h(x_h, \mu_F^2) \otimes \mathbb{C}_{k,q}^{\text{S}}(x_h, \mu_F^2) + D_g^h(x_h, \mu_F^2) \otimes \mathbb{C}_{k,g}^{\text{S}}(x_h, \mu_F^2)] \\ &\quad + \sum_{p=1}^{n_f} \sigma_p^{(0)}(Q^2) D_{\text{NS},p}^h(x_h, \mu_F^2) \otimes \mathbb{C}_{k,q}^{\text{NS}}(x_h, \mu_F^2), \quad \text{for } k = \text{T, L} \\ F_A^h(x_h, Q^2) &= \sum_{p=1}^{n_f} A_p^{(0)}(Q^2) D_{A,p}^h(x_h, \mu_F^2) \otimes \mathbb{C}_{A,q}^{\text{NS}}(x_h, \mu_F^2). \end{aligned} \quad (2.2)$$

The NNLO coefficient functions $C_{k,l}^{\text{S,NS}}$ with $k = T, L, A$ and $l = q, g$ have been calculated in Refs. [42–45]. The renormalization scale for convenience has been set equal to the mass factorization scale μ_F . In Eq. 2.2, $\sigma_p^{(0)}$ is the total cross section for quark production p at LO and $\sigma_{\text{tot}}^{(0)}$ is the corresponding sum over all active flavors n_f , $\sigma_{\text{tot}}^{(0)} = \sum_p \sigma_p^{(0)}$, while $A_p^{(0)}$ is the asymmetry factor to which only non-singlet channel partonic subprocesses can contribute. In our analysis, we set n_f to 5. In the formulae 2.2, symbol \otimes also denotes the standard convolution integral, defined as

$$f(z) \otimes g(z) = \int_0^1 dx \int_0^1 dy f(x)g(y)\delta(z - xy), \quad (2.3)$$

and we have defined the singlet (S) and non-singlet (NS, A) combinations of quark fragmentation functions. These are given by

$$D_S^h(x_h, \mu_F^2) = \frac{1}{n_f} \sum_p [D_p^h(x_h, \mu_F^2) + D_{\bar{p}}^h(x_h, \mu_F^2)], \quad (2.4)$$

$$D_{\text{NS},p}^h(x_h, \mu_F^2) = D_p^h(x_h, \mu_F^2) + D_{\bar{p}}^h(x_h, \mu_F^2) - D_S^h(x_h, \mu_F^2), \quad (2.5)$$

$$D_{\text{A},p}^h(x_h, \mu_F^2) = D_p^h(x_h, \mu_F^2) - D_{\bar{p}}^h(x_h, \mu_F^2). \quad (2.6)$$

where dependence of the $D_p^h(x_h, \mu_F^2)$ and $D_g^h(x_h, \mu_F^2)$ in Eq. 2.2 on μ_F follows the Dokshitzer-Gribov-Lipatov-Altarelli-Parisi (DGLAP) evolution equation with time-like splitting kernels. The time-like splitting functions have been calculated up to $\mathcal{O}(\alpha_s^3)$ in the strong coupling constant and can be found in Refs. [46–51]. As in the case of SIA, the differential decay width for the $H \rightarrow gg$ process in the heavy-top limit is given by

$$\frac{d\Gamma^h}{dx_h} = \Gamma_0 \left(D_S^h(x_h, \mu_F^2) \otimes \mathbb{C}_q(x_h, \mu_F^2) + D_g^h(x_h, \mu_F^2) \otimes \mathbb{C}_g(x_h, \mu_F^2) \right). \quad (2.7)$$

where Γ_0 is the LO decay width for this process in the heavy-top limit and the coefficient function $\mathbb{C}_{q/g}(x_h, \mu_F^2)$ can be obtained by appropriately processing those of a scalar with a generic $\phi G^{\mu\nu} G_{\mu\nu}$ coupling, and have been calculated up to NNLO [48, 52]. In this work, we focus on the analysis carried out at NLO in QCD.

Concerning the theoretical calculations employed here, given that the present study is based on pseudo-data, it is not necessary to account for higher-order QCD effects or electroweak corrections. Indeed, by far the dominant contribution to the FFs sensitivity of various processes at future lepton colliders is contained within the NLO calculation. Moreover, we are only interested in the relative reduction of the FFs uncertainties once the data from future lepton colliders is included in the fit.

The NLO QCD predictions of the described above processes are calculated with the FMNLO program [37], which enables fast convolution with FFs using stored grids on hard coefficient functions. The central values of the pseudo-data initially coincide with the corresponding prediction obtained using this NLO calculation with

| x_h Range | $\delta_{\text{sys}}^{\text{exp}}$ [%] | x_h Range | $\delta_{\text{sys}}^{\text{exp}}$ [%] | x_h Range | $\delta_{\text{sys}}^{\text{exp}}$ [%] |
|-------------|--|-------------|--|-------------|--|
| 0.014–0.016 | 32 | 0.077–0.082 | 6.0 | 0.274–0.296 | 1.9 |
| 0.016–0.022 | 7.3 | 0.082–0.088 | 6.0 | 0.296–0.318 | 1.8 |
| 0.022–0.027 | 3.7 | 0.088–0.099 | 5.9 | 0.318–0.351 | 1.9 |
| 0.027–0.033 | 2.7 | 0.099–0.110 | 5.7 | 0.351–0.384 | 2.3 |
| 0.033–0.038 | 2.4 | 0.110–0.121 | 5.5 | 0.384–0.417 | 2.6 |
| 0.038–0.044 | 2.5 | 0.121–0.143 | 6.4 | 0.417–0.450 | 3.2 |
| 0.044–0.049 | 3.0 | 0.143–0.164 | 9.6 | 0.450–0.482 | 3.4 |
| 0.049–0.055 | 3.0 | 0.164–0.186 | 15 | 0.482–0.526 | 3.8 |
| 0.055–0.060 | 3.7 | 0.186–0.208 | 15 | 0.526–0.570 | 4.3 |
| 0.060–0.066 | 4.4 | 0.208–0.230 | 6.6 | 0.570–0.658 | 4.9 |
| 0.066–0.071 | 5.3 | 0.230–0.252 | 3.3 | 0.658–0.768 | 5.6 |
| 0.071–0.077 | 5.5 | 0.252–0.274 | 2.3 | 0.768–1.000 | 14 |

Table 1. The binning and the corresponding uncorrelated systematic (relative) error for the charged kaon distribution of the scaled momentum measured in SLD.

the NPC23 set [9, 10] as input. Subsequently, the central values are subjected to fluctuations in accordance with the corresponding experimental uncertainties. This implies that, by construction, one should find $\chi^2/N_{\text{pt}} \simeq 1$ from the fit to the pseudo-data. Statistical uncertainties are evaluated from the expected number of events per bin and systematic uncertainties are set to be those of the baseline measurement from SLD at Z -pole [23]. The identified π^\pm , K^\pm and p/\bar{p} production in hadronic Z boson decays are measured in SLD. In addition to flavor-inclusive Z boson decays, measurements are made for Z boson decays into light (u, d, s), c , and b primary flavors. However, the majority of the focus is on the systematic uncertainties associated with the production of π^\pm , K^\pm and p/\bar{p} . Table 1 presents the binning and the corresponding uncorrelated systematic (relative) error for the charged kaon distribution of the scaled momentum, as measured in SLD. The correlated systematic (relative) error is 1%. Table 1 reveals that the uncorrelated systematic error ranges from 1.8% to 32%.

We now proceed to present pseudo-data generation. If σ_i^{th} is the theoretical cross-section for bin i of a given process, then the central values of the pseudo-data σ_i^{exp} is constructed by means of

$$\sigma_i^{\text{exp}} = \sigma_i^{\text{th}} \times (1 + r_i \cdot \delta_{\text{tot},i}^{\text{exp}} + s \cdot \delta_{\text{cor}}^{\text{exp}}) \quad (2.8)$$

where r_i and s are univariate Gaussian random numbers, while $\delta_{\text{tot},i}^{\text{exp}}$ denotes the total (relative) experimental uncertainty associated with this specific bin. Further-

more, $\delta_{\text{cor}}^{\text{exp}}$ represents correlated systematic uncertainties, which are identical across all pseudo-data bins of lepton collider experiments and $\delta_{\text{cor}}^{\text{exp}} = 1\%$.

In Eq. (2.8), the total experimental uncertainty $\delta_{\text{tot},i}^{\text{exp}}$ is defined as

$$\delta_{\text{tot},i}^{\text{exp}} \equiv \left((\delta_{\text{stat},i}^{\text{exp}})^2 + (\delta_{\text{sys},i}^{\text{exp}})^2 \right)^{1/2}. \quad (2.9)$$

In this expression, the relative statistical error $\delta_{\text{stat},i}^{\text{exp}}$ is computed as

$$\delta_{\text{stat},i}^{\text{exp}} = (N_{\text{ev},i})^{-1/2} \quad (2.10)$$

where $N_{\text{ev},i} = \sigma_i^{\text{th}} \times \mathcal{L}$ is the expected number of events in bin i with \mathcal{L} being luminosity for various processes. In Eq. (2.9), $\delta_{\text{sys},i}^{\text{exp}}$ indicates the uncorrelated systematic error of bin i , which is derived from the reference SLD measurement at Z -pole.

In Table 2 we present the summary of the main features of the CEPC, FCC- ee , and ILC pseudo-data generated for the present study, respectively. For each process, we indicate the center-of-mass energy, luminosity (number of events), final state, kinematic cuts, the identified hadrons, and finally the number of data points after data selection. The expected integrated luminosities refer to the total luminosity over the entire run period, summed over two interaction points. For simplicity, the binning and the systematic uncertainties of the pseudo-data for the final state hadrons being h^+ , h^- and h^\pm , such as π^+ , π^- and π^\pm , are identical and set to be those of the corresponding identified hadron, such as π^\pm , production measured in SLD. Moreover, the anticipated number of events per bin for inclusive $q\bar{q}$ production with $\cos(\theta) > 0$ cut must be multiplied by two, due to the contribution from $\cos(\theta) < 0$. A similar situation arises in $W^-W^{+,*}$ production because of the contribution from $W^+W^{-,*}$ production. In Table 2, we combine the expected number of events for $W^-W^{+,*}$ production at 160 GeV and above based on the LO cross section, which we then use as the total events at 160 GeV.

It is finally necessary to mention that we have implemented stringent selection criteria on hadron kinematics, requiring both the hadron energy fraction $x_h > 0.01$ and the hadron energy $E_h > 4$ GeV, to ensure the validity of leading-twist factorization and the convergence of perturbative calculations. The hadron energies are measured in the center-of-mass frame and the virtual W^* boson rest frame for quark pair production and $W^-W^{+,*}$ production, respectively. In the case of Higgs boson decay, the Higgs boson rest frame is selected as the reference frame.

2.3 Theoretical setup and fit of FFs

The parameterization form of fragmentation functions to charged hadrons used at the initial scale Q_0 is

$$xD_{h/i}(x, Q_0) = x^{\alpha_i^h} (1-x)^{\beta_i^h} \exp\left(\sum_{n=0}^m a_{i,n}^h (\sqrt{x})^n\right), \quad (2.11)$$

| e^+e^- annihilation | | | | | | | |
|----------------------------|---------------------------------|-----------|------|-------------------------------------|--------------------|-----------|-----------------|
| \sqrt{s} (GeV) | luminosity (ab^{-1}) | | | final state | kinematic cuts | hadrons | N_{pt} |
| | CEPC | FCC- ee | ILC | | | | |
| 91.2 | 60 | 150 | - | $q\bar{q}$ | $\cos(\theta) > 0$ | $h^{+,-}$ | 132 |
| | | | | $c\bar{c}/b\bar{b}$ | - | h^\pm | 65 |
| 160 | 4.2 | - | - | $q\bar{q}$ | $\cos(\theta) > 0$ | $h^{+,-}$ | 168 |
| | | | | $c\bar{c}/b\bar{b}$ | - | h^\pm | 83 |
| 161 | - | 10 | - | $q\bar{q}$ | $\cos(\theta) > 0$ | $h^{+,-}$ | 168 |
| | | | | $c\bar{c}/b\bar{b}$ | - | h^\pm | 83 |
| 240 | 13 | 5 | - | $q\bar{q}$ | $\cos(\theta) > 0$ | $h^{+,-}$ | 186 |
| | | | | $c\bar{c}/b\bar{b}$ | - | h^\pm | 92 |
| 250 | - | - | 2 | $q\bar{q}$ | $\cos(\theta) > 0$ | $h^{+,-}$ | 186 |
| | | | | $c\bar{c}/b\bar{b}$ | - | h^\pm | 92 |
| 350 | - | 0.2 | 0.2 | $q\bar{q}$ | $\cos(\theta) > 0$ | $h^{+,-}$ | 198 |
| | | | | $c\bar{c}/b\bar{b}$ | - | h^\pm | 98 |
| 360 | 0.65 | - | - | $q\bar{q}$ | $\cos(\theta) > 0$ | $h^{+,-}$ | 198 |
| | | | | $c\bar{c}/b\bar{b}$ | - | h^\pm | 98 |
| 365 | - | 1.5 | - | $q\bar{q}$ | $\cos(\theta) > 0$ | $h^{+,-}$ | 198 |
| | | | | $c\bar{c}/b\bar{b}$ | - | h^\pm | 98 |
| 500 | - | - | 4 | $q\bar{q}$ | $\cos(\theta) > 0$ | $h^{+,-}$ | 198 |
| | | | | $c\bar{c}/b\bar{b}$ | - | h^\pm | 98 |
| W boson decay channels | | | | | | | |
| \sqrt{s} (GeV) | # events (million) | | | final state | kinematic cuts | hadrons | N_{pt} |
| | CEPC | FCC- ee | ILC | | | | |
| 80.419 | 116 | 68 | 62 | $W^-W^{*+} \rightarrow W^-q\bar{q}$ | - | $h^{+,-}$ | 120 |
| | 58 | 34 | 31 | $W^-W^{*+} \rightarrow W^-c\bar{s}$ | | | |
| Higgs boson decay channels | | | | | | | |
| \sqrt{s} (GeV) | # events (million) | | | final state | kinematic cuts | hadrons | N_{pt} |
| | CEPC | FCC- ee | ILC | | | | |
| 125 | 0.23 | 0.09 | 0.07 | gg | - | h^\pm | 77 |
| | 0.08 | 0.03 | 0.02 | $c\bar{c}$ | | | |
| | 1.53 | 0.59 | 0.47 | $b\bar{b}$ | | | |

Table 2. A summary of the main features of the CEPC, FCC- ee , and ILC pseudo—data generated for the present study. For each process, we indicate the center-of-mass energy, luminosity (number of events), final state, kinematic cuts, the identified hadrons, and the number of data points after data selection. Here h^\pm and $h^{+,-}$ denote $(\pi^\pm, K^\pm, p/\bar{p})$ and $(\pi^+, \pi^-, K^+, K^-, p, \bar{p})$, respectively.

where $\{\alpha, \beta, a_n\}$ are free parameters in the fit, and i and h indicate the flavor of the parton and the hadron, respectively. We choose $Q_0 = 5 \text{ GeV}$ and use a zero-

mass scheme for heavy quarks. One advantage of the above parametrization form is that the fragmentation functions are positively defined, thus no additional positivity constraints need to be applied. The total number of free parameters is 63 for π^+ , K^+ and p combined. Further details can be found in Ref. [10]. Furthermore, the FFs of negative-charged hadrons are related to those of positive-charged hadrons via charge conjugation. The fragmentation functions are evolved to higher scales using two-loop time-like splitting kernels to be consistent with the NLO analysis. The splitting functions were calculated in Refs. [53] and are implemented in HOPPET [54, 55] which we use in the analysis.

The quality of the agreement between new experimental measurements and the corresponding theoretical predictions for a given set of fragmentation parameters is quantified by the log-likelihood function (χ^2), which is given by [56]

$$\chi^2(\{\alpha, \beta, a_n\}, \{\lambda\}) = \sum_{k=1}^{N_{\text{pt}}} \frac{1}{s_k^2} \left(D_k - T_k - \sum_{\mu=1}^{N_\lambda} \sigma_{k,\mu} \lambda_\mu \right)^2 + \sum_{\mu=1}^{N_\lambda} \lambda_\mu^2. \quad (2.12)$$

N_{pt} is the number of data points, s_k^2 is the total uncorrelated uncertainties by adding statistical and uncorrelated systematic uncertainties in quadrature, D_k is the central value of the experimental measurements, and T_k is the corresponding theoretical prediction which depends on $\{\alpha, \beta, a_n\}$. $\sigma_{k,\mu}$ are the correlated errors from source μ (N_λ in total). We assume that the nuisance parameters λ_μ follow a standard normal distribution.

By minimizing $\chi^2(\{\alpha, \beta, a_n\}, \{\lambda\})$ with respect to the nuisance parameters, we get the profiled χ^2 function

$$\chi^2(\{\alpha, \beta, a_n\}, \{\hat{\lambda}\}) = \sum_{i,j=1}^{N_{\text{pt}}} (T_i - D_i) [\text{cov}^{-1}]_{ij} (T_j - D_j), \quad (2.13)$$

where cov^{-1} is the inverse of the covariance matrix

$$(\text{cov})_{ij} \equiv s_i^2 \delta_{ij} + \sum_{\mu=1}^{N_\lambda} \sigma_{i,\mu} \sigma_{j,\mu}, \quad (\text{cov}^{-1})_{ij} \equiv \frac{\delta_{ij}}{s_i^2} - \sum_{\mu,\nu=1}^{N_\lambda} \frac{\sigma_{i,\mu}}{s_i^2} A_{\mu\nu}^{-1} \frac{\sigma_{j,\nu}}{s_j^2}. \quad (2.14)$$

The symbol $A_{\mu\nu}$ is defined as

$$A_{\mu\nu} = \delta_{\mu\nu} + \sum_{k=1}^{N_{\text{pt}}} \frac{\sigma_{k,\mu} \sigma_{k,\nu}}{s_k^2}. \quad (2.15)$$

We neglect correlations of experimental uncertainties between different data points since they are not available. However, we include theoretical uncertainties into the covariance matrix of Eq. (2.14) by default, assuming these to be fully correlated

among points in each subset of the data shown in Table 2. The theoretical uncertainties $\sigma_{j,\mu}$ are estimated by the half-width of the envelope of theoretical predictions based on 9 scale combinations, namely $\mu_F/\mu_{F,0} = \mu_R/\mu_{R,0} = \{1/2, 1, 2\}$ and $\mu_D/\mu_{D,0} = \{1/2, 1, 2\}$ where μ_R and μ_D is the renormalization and fragmentation scales, respectively. The central values of these scales, namely $\mu_{F,0}$, $\mu_{R,0}$ and $\mu_{D,0}$, are set to the center-of-mass energy, \sqrt{s} , for both inclusive $q\bar{q}$ production and Higgs boson decay processes. In the case of $W^-W^{+,*}$ production, the values of $\mu_{F,0}$ and $\mu_{R,0}$ are set to the mass of the W boson, m_W . However, the value of $\mu_{D,0}$ is set to the invariant mass of an off-shell W boson.

The best-fit fragmentation parameters are determined by minimizing the χ^2 and then further validated through a series of profile scans on each of those parameters. These parameter space scans are conducted using the MINUIT [57] program. We apply a tolerance criterion of $\Delta\chi^2 \sim 1$ to determine parameter uncertainties. Additionally, we employ the iterative Hessian approach [58] to generate error sets of fragmentation functions, which can then be used to propagate parameter uncertainties to physical observables.

3 Results and discussions

In this section, we utilize the set of pseudo-data enumerated in Table 2 to generate various parton FFs to three light charged hadrons and assess the extent to which these pseudo-data constrain the FFs. Subsequently, we conduct an alternative fit to evaluate the impact of theoretical uncertainties on the extracted FFs. Finally, we discuss each jet of three-jet events originating from hadronic Z decays.

3.1 The constraints to FFs from future lepton colliders

We first present the results from CEPC. The total χ^2 is 1659.2 for a total number of data points of 1831, resulting in $\chi^2/N_{\text{pt}} = 0.91$, which is not unexpected and has been explained in subsection 2.2. A comparison of the baseline NPC23 FFs with those based on CEPC pseudo-data at the scale $Q_0 = 5 \text{ GeV}$ is presented in Figure 2. For simplicity, only the FFs for various partons fragmenting into π^+ , K^+ , and p are shown. The FFs for negative charge hadrons are obtained through charge conjugation. In each row, the sub-figures in the left column show the FFs of the constituent quarks to the charged hadrons, namely the u and \bar{d} quarks to π^+ , the u and \bar{s} quarks to K^+ , and the u and d quarks to p . The remaining sub-figures correspond to FFs of un-favored quarks and gluon, as well as c and b quarks to the identified hadrons, respectively. Both the absolute values of momentum fraction times the FFs and their ratios, normalized to the central values of the NPC23 baseline, are shown. In this comparison, the colored band represents the associated uncertainties estimated with the Hessian Method at the 68% confidence level (C.L.).

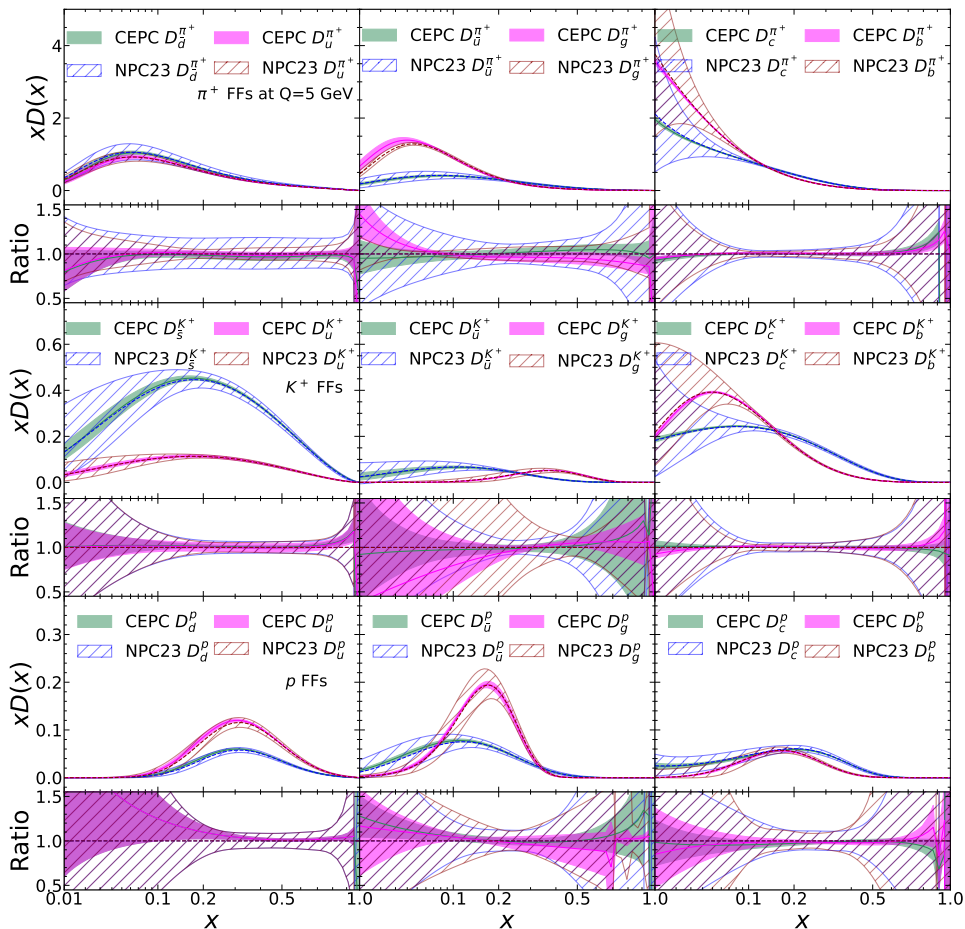


Figure 2. A comparison of our fragmentation functions to those of NPC23 on the diverse outcomes of parton fragmentation, including π^+ , K^+ , and p , at an energy of 5 GeV. The colored band represents the uncertainties estimated with the Hessian Method at the 68% confidence level, with their ratios normalized to the central value of the baseline from the NPC23 study displayed in the lower panel of each subplot.

As anticipated, the central values of the NPC23 and our fit exhibit a good agreement, spanning a broad range of x values in all cases. This can be clearly observed in the lower panel of each figure. For the quarks fragmenting into light charged hadrons, we observe a marked reduction in the FFs uncertainties. This is of particular significance for the c and b quarks, for the reason that a considerable number of measurements from heavy-flavor tagged hadronic events in e^+e^- collisions have strong constraints to heavy quark FFs. In the cases of the valence quarks and sea quarks, there is a reduction in the FFs uncertainties across a wide range of x . The primary reason for this improvement is the increased statistics and the diverse measurements across a wide range of collision energies, from the Z -pole to 360 GeV, which will be available at the CEPC.

In the case of the gluon, it can be observed that the CEPC results for the gluon fragmenting into K^+ and p also exhibit notable reduced FFs uncertainties across the entire kinematic region, in comparison to the NPC23 results. The FFs to π^+ from gluon have reduced uncertainties at $x > 0.08$. These results highlight the importance of the measurements for the $H \rightarrow gg$ channel which represent a unique handle on the poorly known gluon content of three light charged hadrons in our work. Furthermore, we observe a slight increase of uncertainties for gluon FF to π^+ in the small x region, as is evident from the lower ratio plot. This can be attributed to the insufficient number of data points available for the determination of gluon FFs to π^+ after data selection in the small x region.

In Figure 3, we present a comparison of the symmetric relative errors between the π^+ , K^+ and p FF from CEPC and NPC23 at the scale $Q_0 = 5 \text{ GeV}$. From Figure 3, it can be seen that the range of values shown on the plot is $0.01 < x < 0.9$ to avoid numerical result oscillations caused by the LHgrid interpolation in the endpoint region. In the case of π^+ FFs, the relative errors observed in our CEPC study are considerably smaller than those observed in the NPC23 FFs, with the exception of the FFs to π^+ from gluon in the small x region, which has been previously explained. For instance, the relative errors for the valence quark, \bar{d} , are reduced by approximately a factor of five, from approximately 20% to a few percent, in a wide region of x . Furthermore, we observe a pronounced reduction in the symmetric relative errors for the FFs to K^+ and p . This is particularly significant in the small and large x regions. The relative errors for the valence quarks u and d fragmenting into p are identical for the reason that we have assumed exact flavor symmetry between the two valence quarks $D_u^p(x, Q_0) = 2 D_d^p(x, Q_0)$ at the starting scale Q_0 .

We now present in Figure 4 a comparison of the relative errors among the FFs obtained from CEPC, FCC- ee , and ILC measurements, respectively, at the scale $Q_0 = 5 \text{ GeV}$. It can be observed that the pseudo-data from CEPC and FCC- ee have a comparable impact on the uncertainties associated with the FFs. This is due to the fact that the differing integrated luminosities at different processes did not result in any apparent effects on the FFs. In the case of ILC, the constraints on the π^+ and K^+ FFs are comparable to those observed in the CEPC case. However, there are stronger constraints on the π^+ FFs from gluon and K^+ FFs from the \bar{u} quark in the small x region, in comparison to the CEPC. For the p FFs, it can be observed that the relative errors of the FFs fitted through ILC measurements are larger than those from CEPC in the entire region of x , particularly in the small x region.

3.2 Alternative fit

In this subsection, we utilize the FFs from CEPC as a case study to investigate the impact of individual data sets and the influence of theoretical uncertainties on the extracted FFs. By comparing these alternative fits with the baseline fit derived from the complete data sets presented in Table 2, we aim to identify potential constraints

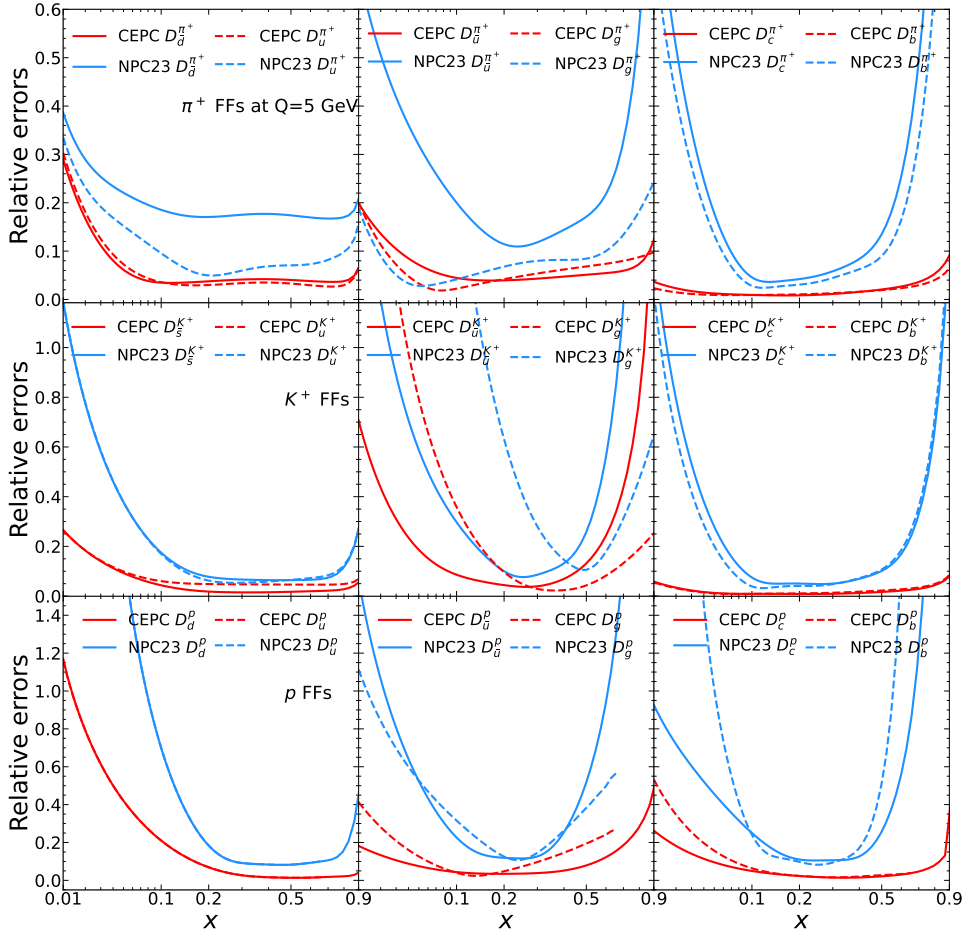


Figure 3. A comparison of the symmetric relative errors between the π^+ , K^+ and p fragmentation functions from the CEPC and the NPC23 sets.

between different data sets and the influence of higher-order QCD effects. To evaluate the impact of particular data sets on distinct fragmentation processes, alternative fits are conducted by systematically excluding a specific group of subsets at a time and re-fitting the FFs at NLO. Throughout the fitting process, all other variables are maintained consistent with the baseline fit, including the kinematic cuts and the treatment of theoretical uncertainties.

A comparison of the relative errors of the global fit for the π^+ , K^+ and p FFs and a refitted version, which excludes a specific group of subsets from the full set, is presented in Figure 5. Upon the removal of the $W^-W^{+,*}$ production data set, it becomes evident that the relative errors for the FFs of light (anti) quarks are larger than those of the baseline fit. This is particularly significant for the FFs to π^+ . Additionally, it is observed that the relative errors for the FFs of heavy quarks (c and b) and gluon remain almost unchanged throughout the entire region depicted in the plot. This stability is to be expected, given that the data sets from the heavy-

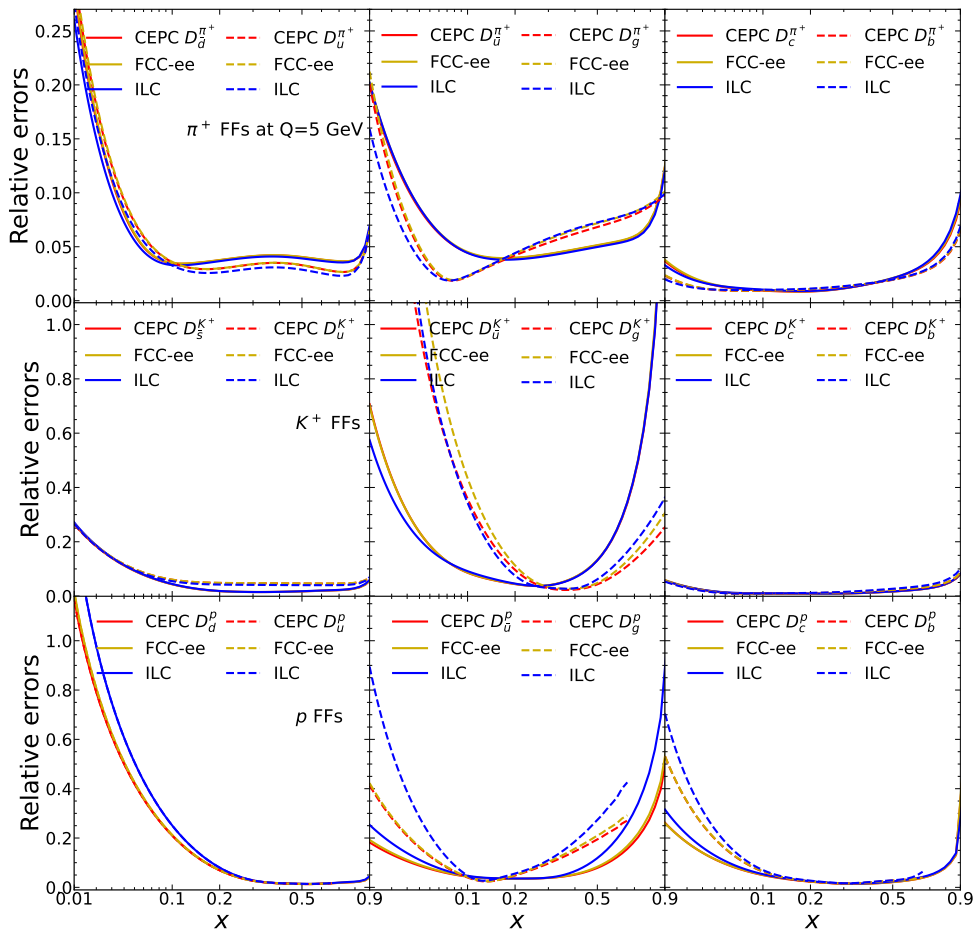


Figure 4. A comparison of the relative errors among the FFs obtained from CEPC, FCC- ee and ILC measurements, respectively, at the scale $Q_0 = 5$ GeV.

flavor tagged measurements of $e^+e^- \rightarrow c\bar{c}/b\bar{b}$ and $H \rightarrow c\bar{c}/b\bar{b}$ processes can lead to well-constrained FFs from heavy flavor. Upon the removal of the data sets from the Higgs boson decay processes, it is evident that the measurements from the decay of the Higgs boson exert a profound influence on the FFs of gluon. This is because the data from the $H \rightarrow gg$ process represents a unique channel through which the fragmentation of gluons into three light charged hadrons can be understood within the context of the complete data set, as presented in Table 2. Furthermore, a slight increase in the relative error for heavy quark FFs in the small x region is observed. This is a consequence of the exclusion of data from the $H \rightarrow c\bar{c}/b\bar{b}$ processes.

The data sets on quark pair production at lepton colliders show a larger impact compared to the $W^-W^{+,*}$ production data set for the FFs of light quarks. This is reflected in the curve labelled (w/o W and H) above the curve labelled (w/o W) in Figure 5. Furthermore, it can be observed that the relative errors for the FFs to light charged hadrons from heavy quarks labelled (w/o W and H) are slightly larger

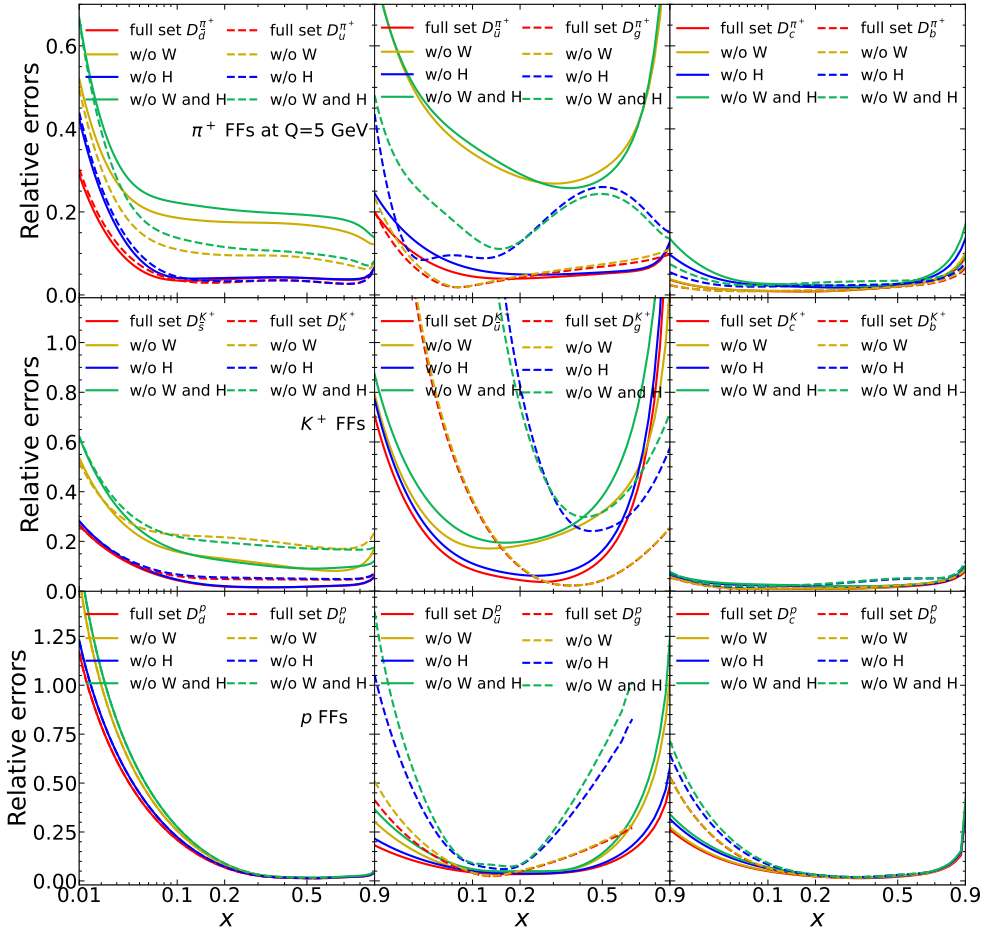


Figure 5. A comparison of the global fit for the π^+ , K^+ and p fragmentation function and a refitted version by excluding a specific group of subsets from the full set presented in Table 2.

than those of the baseline fit, particularly in the small x region. This is analogous to the situation observed after subtracting data sets from Higgs boson decay processes.

We now turn to study the effect of the higher-order QCD corrections on the FFs to light charged hadrons. We first show in Figure 6 the distribution of the hadron energy fraction for inclusive $q\bar{q}$ production at 160 GeV, and for Higgs boson decaying into gluons, where the partons subsequently undergo fragmentation to produce the identified hadrons π^+ . The FFs set used for the evaluation of various order predictions is NPC23_P1p_nlo. The calculation of NNLO corrections using FMNLO is presented in Appendix A. The color bands represent scale uncertainties.

Figure 6 illustrates that the NLO prediction exhibits a significantly reduced scale uncertainty in comparison to the LO prediction across the entire region of x . The inclusion of NNLO corrections results in a further reduction in scale uncertainties. It is observed that the error bands at NLO even encompass those at NNLO in the

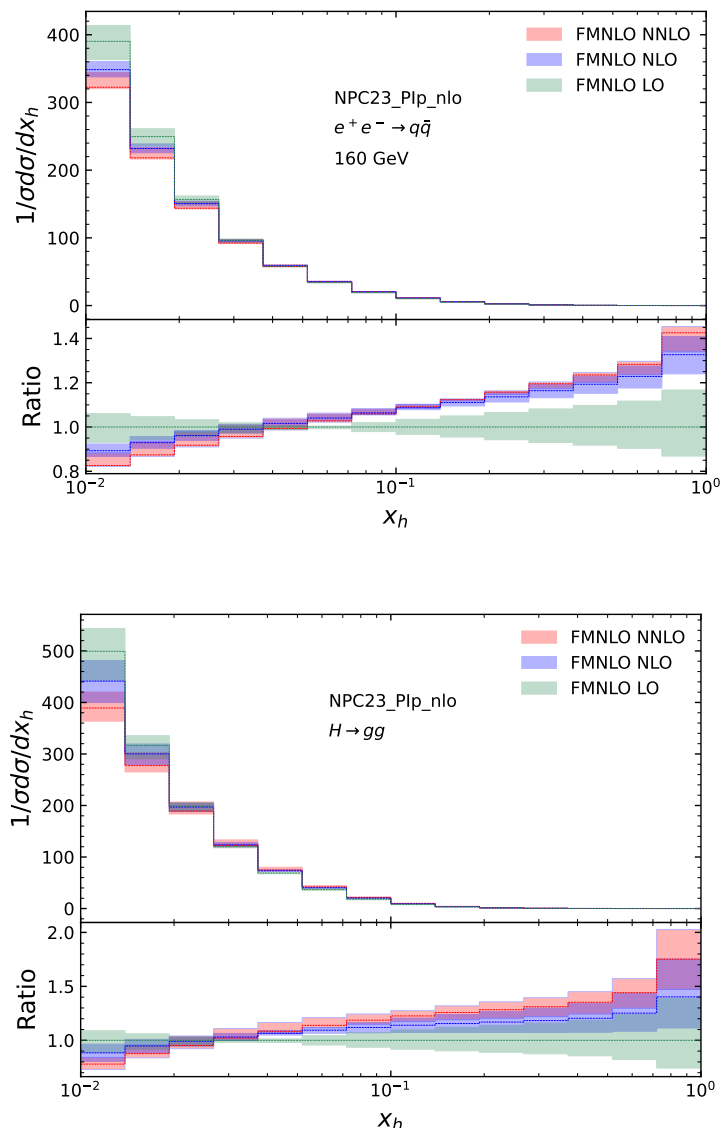


Figure 6. The distribution of the hadron energy fraction from FMNLO at various orders for electron-positron annihilation at a center-of-mass energy of 160 GeV, and for Higgs boson decaying into gluons. In the lower panel, the ratio to the central value at LO is presented. The error bands represent the scale uncertainties.

intermediate x region for the inclusive $q\bar{q}$ production. Furthermore, the resulting predictions using the NNFF10_PIp_nnlo set, as presented in Ref. [12], are comparable to those obtained using the NPC23_PIp_nlo set. Consequently, alternative fits were conducted without including the theoretical uncertainties to discuss the effects of the higher-order corrections. All resulting FFs are compared to the baseline fit including the theoretical uncertainties and their ratios are shown in Figure 7. The colored band represents the associated uncertainties estimated with the Hessian Method at the 68% confidence level.

As illustrated in Figure 7, we find that excluding theoretical uncertainties has a significant impact on the reduction of FFs uncertainties, with the error bands nearly within the Hessian uncertainties of the baseline fit. For the case of the favored

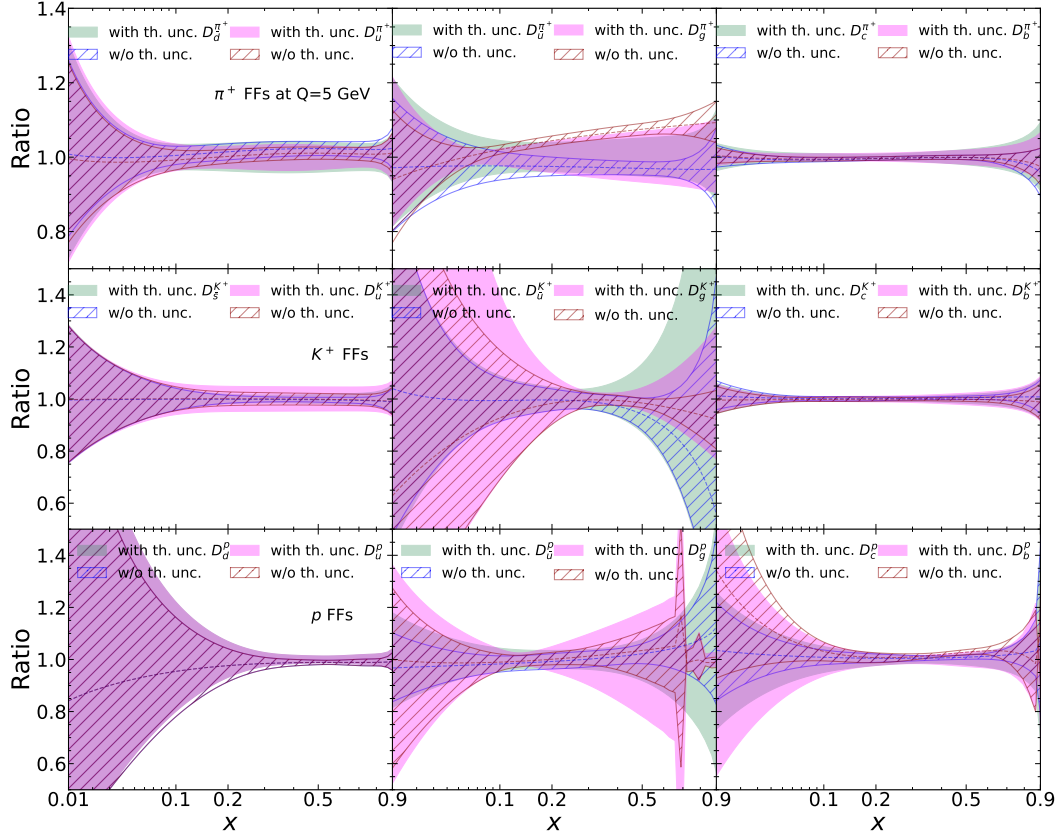


Figure 7. A comparison between the baseline fit, including the theoretical uncertainties, and a refitted version that excludes the theoretical uncertainties.

quark, the error bands excluding theoretical uncertainties exhibit a reduced uncertainty compared to those including them. For instance, the Hessian uncertainties for the \bar{d} quark fragmenting into π^+ and the u quark fragmenting into the K^+ are approximately two times smaller than those of the baseline fit. For the sub-figures in the second column, the error bands excluding theoretical uncertainties are considerably smaller than those of the baseline fit, as is evident in the large region of x . In the case of heavy quarks, the reduced uncertainties are reasonable, as is evident from the FFs to the proton and π^+ in a wide kinematic range. Furthermore, Figure 8 presents a comparison of the relative errors among the FFs obtained from CEPC, FCC- ee , and ILC measurements without including theoretical uncertainties. In comparison to the fits presented in Figure 4, the corresponding results in Figure 8 are shifted downwards in the plot, indicating a stronger constraint on the FFs when higher-order corrections are included in the global QCD fit. Consequently, the evaluation of NNLO QCD corrections for relevant processes is essential if one is to achieve a precise extraction of the FFs to light charged hadrons at NNLO accuracy.

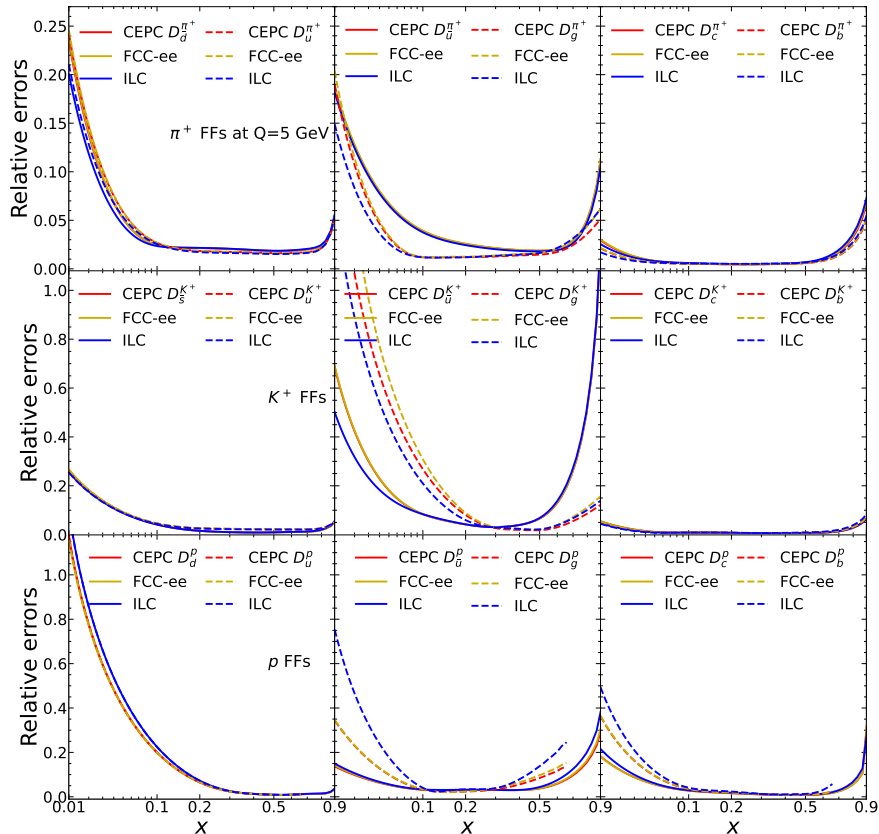


Figure 8. Similar to Figure 4, but excluding theoretical uncertainties in fit of FFs.

3.3 The constraints from three-jet production

The present study is primarily concerned with inclusive hadronic production at lepton colliders. Nevertheless, the experiment is also capable of measuring the relevant observable in three-jet production. In three-jet events, where the jets are ordered according to their energies, the first two jets are enriched in quarks and the third in gluons. In this manner, the fragmentation of gluons can be investigated through the examination of the momentum spectrum of the lowest-energy jet (enriched in gluons) in three-jet events.

In a manner analogous to the approach employed by the ALEPH Collaboration in measuring the jets of three-jet events from hadronic Z decays, the jets are clustered using the k_{\perp} (Durham) algorithm with the E recombination scheme and a jet resolution parameter of $y_{cut} = 0.01$. It is required that the polar angle between each jet and the beam axis be between 30° and 150° . Figure 9 presents a comparison between scale and Hessian uncertainties for the distribution of the hadron energy fraction in each jet of three-jet events, ordered according to their energies. The fragmentation functions employed in this analysis are those derived from the NPC23_PIp_nlo set. The color bands represent the scale uncertainties, while the error bars indicate the Hessian uncertainties. It can be observed that the NLO result for each jet of three-

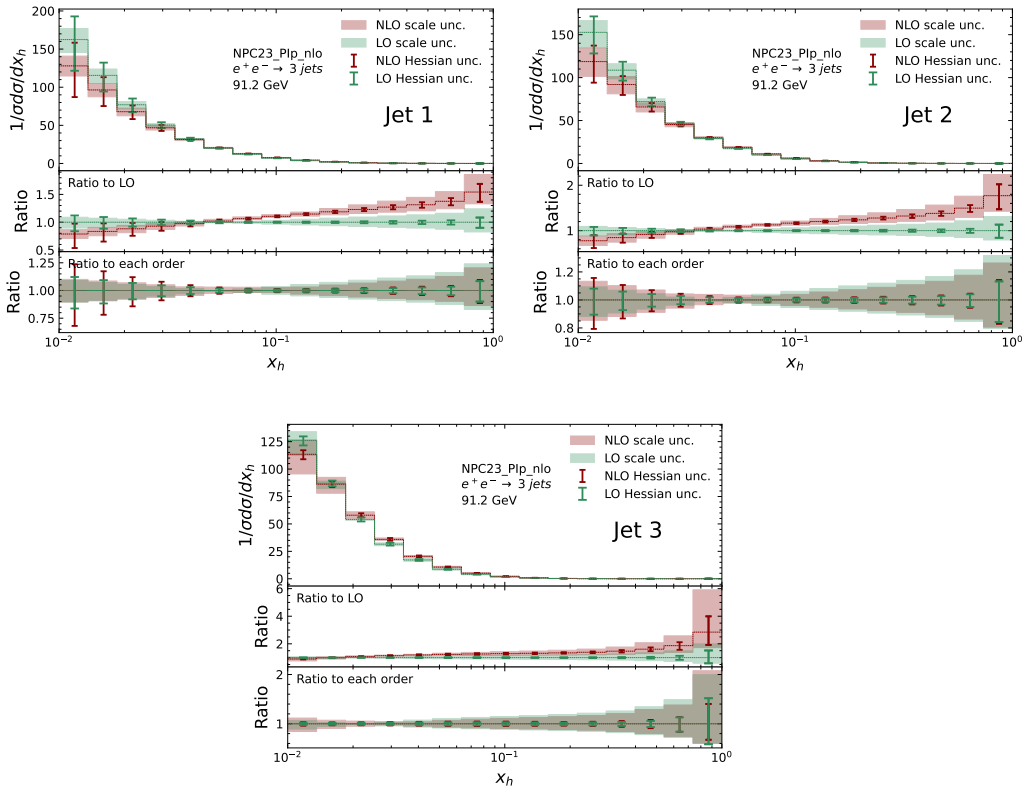


Figure 9. A comparison between the scale uncertainties and the Hessian uncertainties for the distribution of the hadron energy fraction with a center-of-mass energy of 91.2 GeV in each jet of three-jet events. The jets were ordered according to their energies, with the upper-left, upper-right, and second-row plots, respectively. In the last two panels of each plot, the ratio to the central value at LO and the corresponding order are presented, respectively. The color bands represent scale uncertainties, while the error bars indicate Hessian uncertainties.

jet events exhibits a slightly reduced scale uncertainty compared to the LO result in the large x region. However, it is notable that there is an unusual increase in scale uncertainty in the small x region, as is evident from the final panel of each plot in Figure 9. This phenomenon can be attributed, at least in part, to the fact that the scale uncertainty at the LO level is influenced solely by the fragmentation scale, whereas the NLO level is additionally affected by the renormalization scale.

In the case of the first two jets, it can be demonstrated that the Hessian uncertainties are larger than the scale uncertainties in the small x region. Moreover, as the value of x increases, the scale error band gradually encompasses the Hessian error bar. In the case of the lowest-energy jet in three-jet events, the scale uncertainties exceed the Hessian uncertainties across the entire x region depicted in the plot. This observation is evident in the second panel of each plot in Figure 9. The ALEPH Collaboration has measured the inclusive cross section for various particles in three-

jet events, and both systematic and statistical errors are relatively large. This is reported in Ref. [59]. Nevertheless, it is anticipated that the corresponding error will be significantly reduced in future lepton colliders. Consequently, when a global fit including the data from three-jet events is performed to further enhance the understanding of the FFs of partons, particularly those of gluon fragmenting into π^\pm , K^\pm and p/\bar{p} , it is necessary to calculate higher-order corrections for three-jet production at electron-positron colliders.

4 Summary

In this work, we have studied the constraints that future lepton colliders will impose on the FFs to light charged hadrons from quarks and gluon in the framework of QCD collinear factorization. We find the data from CEPC has the potential to significantly reduce the uncertainties of FFs in a wide kinematic region, especially for quark FFs. For example, the relative errors of FFs for the constituent quark \bar{d} fragmenting to π^+ are reduced by almost a factor 5, from around 20% to a few percents, in a wide range of momentum fraction, compared to those from NPC23 global analyses based on current world data. For gluon FF, we observe improvements of uncertainties to all charged hadrons, except for gluon fragmenting to π^+ in the small x region due to our selection cuts. We also study the cases of FCC- ee and ILC, and the conclusions on reduction of FF uncertainties are almost the same as those of CEPC.

We have conducted alternative fits by systematically excluding a specific group of subsets at a time and re-fitting the FFs, to assess the influence of specific data sets on distinct fragmentation processes. Taking the fit for CEPC as an example, we find the measurements of W^-W^{+*} production impose strong constraints to the FFs of light (anti-)quarks while having no effects on gluon FFs. In the case of removal of the Higgs boson decay processes, we find they show a very large impact on the FFs of gluon, which is not so surprising since the data from $H \rightarrow gg$ process is a unique channel to constraining gluon fragmentation to three light charged hadrons among the full data set listed in Table 2. The inclusive two jets production at various center-of-mass energy of course provide the dominant constraints in general.

In addition, we conduct fits without including the theoretical uncertainties to study the impact of higher-order QCD corrections. We observe a significant reduction of the FFs error bands in all cases when excluding theoretical uncertainties. For example, the Hessian uncertainties for \bar{d} quark fragmenting into π^+ and u quark fragmenting into K^+ are about 2 times smaller than those of the baseline fit including the theoretical uncertainties. Therefore, the evaluation of higher-order QCD corrections for all processes shown in Table 2 are necessary for future precision determination of FFs. Currently, the NNLO QCD corrections are available for both SIA and the decay of the Higgs boson to gluons, and have been implemented into the FMNLO program as described in the appendix.

Finally, we discuss the impact of measurements of three-jet production on the FFs, which may further improve the constraints on gluon FFs. By a comparison on the scale variations of theoretical predictions and their uncertainties induced by FFs, we conclude the NNLO corrections will be needed in the future to effectively include the data into a global analysis of FFs.

Acknowledgements

We are grateful to ChongYang Liu for providing the drawing script. The work of JG is supported by the National Natural Science Foundation of China (NSFC) under Grant No. 12275173.

A NNLO calculations in FMNLO

Through this study we have developed v2.1 of the FMNLO program, which allows for NNLO calculations and grid generations for hadron multiplicities in SIDIS, SIA, and decays of the Higgs boson to gluons, that can be found on the website¹. The implementation is based on the analytical results from original calculations in Refs. [42–45, 48, 52, 60, 61]. Instructions on installation and usage of FMNLO can be found in Appedix A of Ref. [37]. Here we highlight only the usage of the NNLO component, which has been available since v2.1. We take the module used for the SIA calculation at NNLO mentioned in subsection 3.2 as an example. This module, named A4001, is one of the default examples available in the FMNLOv2.1 package. The parameter card for this module corresponds to the file FMNLOv2.1/mgen/A4001/proc.run, and reads

```
sidis A4001
# subgrids with name tags
grid siannlo240
pdfname 'CT14nlo'
etag 'e+'
htag 'p'
obs 3
zdef 2
cut 0.02
q2d 10.0
q2u 100000.0
xbjd 0.14
xbju 0.18
yid 0.3
yiu 0.5
```

¹<http://fmnlo.sjtu.edu.cn/~fmnlo/>

```

pdfmember 0
sqrtS 240.0
Rscale 1.0
Fscale 1.0
ncores 30
maxeval 1000000
iseed 11
end

```

where

- `sidis` specifies the name of the directory that contains the module to be loaded.
- `grid` is a string indicating the name of the running job.
- `obs` specifies different observables to be calculated: `3`, `4` is for NNLO calculation of multiplicity distribution in hadron energy fraction for SIA and decays of the Higgs boson to gluons, respectively. For these two cases, parameters from `pdfname` to `htag`, and from `zdef` to `pdfmember` are irrelevant; `2` is for NNLO calculation of multiplicity distribution in hadron scaled momentum (z) for SIDIS. Here `zdef` is irrelevant while other input parameters follow descriptions in appendix of Ref. [10].
- `sqrtS`: the c.m. energy \sqrt{s} or the mass of the Higgs boson in GeV.
- `Rscale`, `Fscale`: ratios of the renormalization and factorization scale w.r.t. our nominal choice of Q . Again `Fscale` is only relevant for SIDIS calculation with `obs=2`.
- `ncores`, `maxeval`, `iseed` indicate technical parameters of numerical calculations, including number of CPU cores used, maximum number of integrand evaluations, and seed for pseudo-random-number generation.

After the grid generation, the multiplicity distributions can be obtained for arbitrary FFs and binnings following the same procedures as described in Ref. [37] for FMNLOv1.0.

B Three-jet production in FMNLO

In FMNLOv2.1 we also include a new module `A5002` for NLO calculation of hadron multiplicity distributions in energy fraction for three-jet production at electron-positron collisions. Note in the calculation the nominal choice of fragmentation scale is set the energy of individual jet while the choice of renormalization scale follows the options in `MG5_aMC@NLO` [62, 63]. This module is tailored for the measurement on

three-jet production from ALEPH collaboration [59] as described in the main text, or from L3 collaboration [64]. Though a general case with different jet algorithms and selection cuts can be implemented easily. The parameter card for this module corresponds to the file `FMNLOv2.1/mgen/A5002/proc.run`, and reads

```
process A5002
# subgrids with name tags
grid trijet1_ag1_e91
obs 1
cut 0.02
ptj1 0.0
ptj2 100.0
# 1/2 for kT or LUCLUS
jalg 1
# 1/2/3 for individual jets ordered in E
ifor 1
# in MG5 format
set ptj 1.0
set lpp1 0
set lpp2 0
set ebeam1 45.59
set ebeam2 45.59
set iseed 11
set muR_over_ref 1.0
set muF_over_ref 1.0
set fixed_ren_scale True
set muR_ref_fixed 91.18
set req_acc_F0 0.002
end
```

The additional parameters compared to similar modules presented in `FMNLOv1.0` are

- `jalg` specifies the jet algorithm and selection cuts used: currently 1, 2 is tailored for the ALEPH and L3 measurements respectively.
- `ifor` indicates the jet to be analysed: can be 1, 2, 3 corresponding to the 1-st, 2-nd, 3-rd jet ordered according to jet energies, namely `ifor = 1` corresponds to the leading jet in energies.

References

- [1] J.C. Collins, D.E. Soper and G.F. Sterman, *Factorization of Hard Processes in QCD*, *Adv. Ser. Direct. High Energy Phys.* **5** (1989) 1 [[hep-ph/0409313](#)].

- [2] J.C. Collins, *Hard scattering factorization with heavy quarks: A General treatment*, *Phys. Rev. D* **58** (1998) 094002 [[hep-ph/9806259](#)].
- [3] A. Metz and A. Vossen, *Parton Fragmentation Functions*, *Prog. Part. Nucl. Phys.* **91** (2016) 136 [[1607.02521](#)].
- [4] D. de Florian, R. Sassot and M. Stratmann, *Global analysis of fragmentation functions for protons and charged hadrons*, *Phys. Rev. D* **76** (2007) 074033 [[0707.1506](#)].
- [5] S. Albino, B.A. Kniehl and G. Kramer, *AKK Update: Improvements from New Theoretical Input and Experimental Data*, *Nucl. Phys. B* **803** (2008) 42 [[0803.2768](#)].
- [6] NNPDF collaboration, *Charged hadron fragmentation functions from collider data*, *Eur. Phys. J. C* **78** (2018) 651 [[1807.03310](#)].
- [7] MAP (MULTI-DIMENSIONAL ANALYSES OF PARTONIC DISTRIBUTIONS) collaboration, *Determination of unpolarized pion fragmentation functions using semi-inclusive deep-inelastic-scattering data*, *Phys. Rev. D* **104** (2021) 034007 [[2105.08725](#)].
- [8] JEFFERSON LAB ANGULAR MOMENTUM (JAM) collaboration, *Simultaneous Monte Carlo analysis of parton densities and fragmentation functions*, *Phys. Rev. D* **104** (2021) 016015 [[2101.04664](#)].
- [9] J. Gao, C. Liu, X. Shen, H. Xing and Y. Zhao, *Simultaneous Determination of Fragmentation Functions and Test on Momentum Sum Rule*, *Phys. Rev. Lett.* **132** (2024) 261903 [[2401.02781](#)].
- [10] J. Gao, C. Liu, X. Shen, H. Xing and Y. Zhao, *Global analysis of fragmentation functions to charged hadrons with high-precision data from the LHC*, [2407.04422](#).
- [11] M. Hirai, S. Kumano, T.H. Nagai and K. Sudoh, *Determination of fragmentation functions and their uncertainties*, *Phys. Rev. D* **75** (2007) 094009 [[hep-ph/0702250](#)].
- [12] NNPDF collaboration, *A determination of the fragmentation functions of pions, kaons, and protons with faithful uncertainties*, *Eur. Phys. J. C* **77** (2017) 516 [[1706.07049](#)].
- [13] M. Soleymaninia, M. Goharipour and H. Khanpour, *First QCD analysis of charged hadron fragmentation functions and their uncertainties at next-to-next-to-leading order*, *Phys. Rev. D* **98** (2018) 074002 [[1805.04847](#)].
- [14] M. Soleymaninia, M. Goharipour and H. Khanpour, *Impact of unidentified light charged hadron data on the determination of pion fragmentation functions*, *Phys. Rev. D* **99** (2019) 034024 [[1901.01120](#)].
- [15] M. Soleymaninia, M. Goharipour, H. Khanpour and H. Spiesberger, *Simultaneous extraction of fragmentation functions of light charged hadrons with mass corrections*, *Phys. Rev. D* **103** (2021) 054045 [[2008.05342](#)].
- [16] I. Borsa, R. Sassot, D. de Florian, M. Stratmann and W. Vogelsang, *Towards a*

- Global QCD Analysis of Fragmentation Functions at Next-to-Next-to-Leading Order Accuracy*, *Phys. Rev. Lett.* **129** (2022) 012002 [[2202.05060](#)].
- [17] MAP (MULTI-DIMENSIONAL ANALYSES OF PARTONIC DISTRIBUTIONS) collaboration, *Pion and kaon fragmentation functions at next-to-next-to-leading order*, *Phys. Lett. B* **834** (2022) 137456 [[2204.10331](#)].
- [18] TASSO collaboration, *Pion, Kaon and Proton Cross-sections in e^+e^- Annihilation at 34-GeV and 44-GeV Center-of-mass Energy*, *Z. Phys. C* **42** (1989) 189.
- [19] TPC/TWO GAMMA collaboration, *Charged hadron inclusive cross-sections and fractions in e^+e^- annihilation $\sqrt{s} = 29$ GeV*, *Phys. Rev. Lett.* **61** (1988) 1263.
- [20] OPAL collaboration, *Measurement of the production rates of charged hadrons in e^+e^- annihilation at the Z^0* , *Z. Phys. C* **63** (1994) 181.
- [21] ALEPH collaboration, *Inclusive π^{+-} , K^{+-} and $(p, \text{anti-}p)$ differential cross-sections at the Z resonance*, *Z. Phys. C* **66** (1995) 355.
- [22] DELPHI collaboration, *π^{+-} , K^{+-} , p and anti- p production in $Z^0 \rightarrow q \text{ anti-}q$, $Z^0 \rightarrow b \text{ anti-}b$, $Z^0 \rightarrow u \text{ anti-}u$, $d \text{ anti-}d$, $s \text{ anti-}s$* , *Eur. Phys. J. C* **5** (1998) 585.
- [23] SLD collaboration, *Production of π^+ , π^- , K^+ , K^- , p and \bar{p} in Light (uds), c and b Jets from Z^0 Decays*, *Phys. Rev. D* **69** (2004) 072003 [[hep-ex/0310017](#)].
- [24] OPAL collaboration, *Charged particle momentum spectra in e^+e^- annihilation at $s^{**}(1/2) = 192\text{-GeV}$ to 209-GeV* , *Eur. Phys. J. C* **27** (2003) 467 [[hep-ex/0209048](#)].
- [25] DELPHI collaboration, *Charged and identified particles in the hadronic decay of Z^0 bosons and in $e^+e^- \rightarrow q \text{ anti-}q$ from 130-GeV to 200-GeV* , *Eur. Phys. J. C* **18** (2000) 203 [[hep-ex/0103031](#)].
- [26] T. Behnke, J.E. Brau, B. Foster, J. Fuster, M. Harrison, J.M. Paterson et al., eds., *The International Linear Collider Technical Design Report - Volume 1: Executive Summary*, [1306.6327](#).
- [27] P. Bambade et al., *The International Linear Collider: A Global Project*, [1903.01629](#).
- [28] ILC INTERNATIONAL DEVELOPMENT TEAM collaboration, *The International Linear Collider: Report to Snowmass 2021*, [2203.07622](#).
- [29] CEPC STUDY GROUP collaboration, *CEPC Conceptual Design Report: Volume 1 - Accelerator*, [1809.00285](#).
- [30] CEPC STUDY GROUP collaboration, *CEPC Conceptual Design Report: Volume 2 - Physics & Detector*, [1811.10545](#).
- [31] CEPC STUDY GROUP collaboration, *CEPC Technical Design Report – Accelerator (v2)*, [2312.14363](#).
- [32] FCC collaboration, *FCC Physics Opportunities: Future Circular Collider Conceptual Design Report Volume 1*, *Eur. Phys. J. C* **79** (2019) 474.
- [33] FCC collaboration, *FCC-ee: The Lepton Collider: Future Circular Collider Conceptual Design Report Volume 2*, *Eur. Phys. J. ST* **228** (2019) 261.

- [34] FCC collaboration, *FCC-hh: The Hadron Collider: Future Circular Collider Conceptual Design Report Volume 3*, *Eur. Phys. J. ST* **228** (2019) 755.
- [35] H. Liang, Y. Zhu, Y. Wang, Y. Che, C. Zhou, H. Qu et al., *Jet origin identification and measurement of rare hadronic decays of Higgs boson at e^+e^- collider*, [2310.03440](#).
- [36] Y. Zhu, H. Liang, Y. Wang, H. Qu, C. Zhou and M. Ruan, *ParticleNet and its application on CEPC jet flavor tagging*, *Eur. Phys. J. C* **84** (2024) 152 [[2309.13231](#)].
- [37] C. Liu, X. Shen, B. Zhou and J. Gao, *Automated calculation of jet fragmentation at NLO in QCD*, *JHEP* **09** (2023) 108 [[2305.14620](#)].
- [38] LHC HIGGS CROSS SECTION WORKING GROUP collaboration, *Handbook of LHC Higgs Cross Sections: 3. Higgs Properties*, [1307.1347](#).
- [39] LHC HIGGS CROSS SECTION WORKING GROUP collaboration, *Handbook of LHC Higgs Cross Sections: 4. Deciphering the Nature of the Higgs Sector*, [1610.07922](#).
- [40] P. Nason and B.R. Webber, *Scaling violation in e^+e^- fragmentation functions: QCD evolution, hadronization and heavy quark mass effects*, *Nucl. Phys. B* **421** (1994) 473.
- [41] B.R. Webber, *Hadronization*, in *Summer School on Hadronic Aspects of Collider Physics*, pp. 49–77, 11, 1994 [[hep-ph/9411384](#)].
- [42] P.J. Rijken and W.L. van Neerven, *$O(\alpha_s^{**2})$ contributions to the longitudinal fragmentation function in e^+e^- annihilation*, *Phys. Lett. B* **386** (1996) 422 [[hep-ph/9604436](#)].
- [43] P.J. Rijken and W.L. van Neerven, *$O(\alpha_s^{**2})$ contributions to the asymmetric fragmentation function in e^+e^- annihilation*, *Phys. Lett. B* **392** (1997) 207 [[hep-ph/9609379](#)].
- [44] P.J. Rijken and W.L. van Neerven, *Higher order QCD corrections to the transverse and longitudinal fragmentation functions in electron - positron annihilation*, *Nucl. Phys. B* **487** (1997) 233 [[hep-ph/9609377](#)].
- [45] A. Mitov and S.-O. Moch, *QCD Corrections to Semi-Inclusive Hadron Production in Electron-Positron Annihilation at Two Loops*, *Nucl. Phys. B* **751** (2006) 18 [[hep-ph/0604160](#)].
- [46] A. Mitov, S. Moch and A. Vogt, *Next-to-Next-to-Leading Order Evolution of Non-Singlet Fragmentation Functions*, *Phys. Lett. B* **638** (2006) 61 [[hep-ph/0604053](#)].
- [47] S. Moch and A. Vogt, *On third-order timelike splitting functions and top-mediated Higgs decay into hadrons*, *Phys. Lett. B* **659** (2008) 290 [[0709.3899](#)].
- [48] A.A. Almasy, S. Moch and A. Vogt, *On the Next-to-Next-to-Leading Order Evolution of Flavour-Singlet Fragmentation Functions*, *Nucl. Phys. B* **854** (2012) 133 [[1107.2263](#)].

- [49] H. Chen, T.-Z. Yang, H.X. Zhu and Y.J. Zhu, *Analytic Continuation and Reciprocity Relation for Collinear Splitting in QCD*, *Chin. Phys. C* **45** (2021) 043101 [[2006.10534](#)].
- [50] M.-x. Luo, T.-Z. Yang, H.X. Zhu and Y.J. Zhu, *Unpolarized quark and gluon TMD PDFs and FFs at N³LO*, *JHEP* **06** (2021) 115 [[2012.03256](#)].
- [51] M.A. Ebert, B. Mistlberger and G. Vita, *TMD fragmentation functions at N³LO*, *JHEP* **07** (2021) 121 [[2012.07853](#)].
- [52] G. Soar, S. Moch, J.A.M. Vermaseren and A. Vogt, *On Higgs-exchange DIS, physical evolution kernels and fourth-order splitting functions at large x*, *Nucl. Phys. B* **832** (2010) 152 [[0912.0369](#)].
- [53] M. Stratmann and W. Vogelsang, *Next-to-leading order evolution of polarized and unpolarized fragmentation functions*, *Nucl. Phys. B* **496** (1997) 41 [[hep-ph/9612250](#)].
- [54] G.P. Salam and J. Rojo, *A Higher Order Perturbative Parton Evolution Toolkit (HOPPET)*, *Comput. Phys. Commun.* **180** (2009) 120 [[0804.3755](#)].
- [55] G. Salam and J. Rojo, *The HOPPET NNLO parton evolution package*, in *16th International Workshop on Deep Inelastic Scattering and Related Subjects*, p. 42, 7, 2008, DOI [[0807.0198](#)].
- [56] J. Gao, L. Harland-Lang and J. Rojo, *The Structure of the Proton in the LHC Precision Era*, *Phys. Rept.* **742** (2018) 1 [[1709.04922](#)].
- [57] F. James and M. Roos, *Minuit: A System for Function Minimization and Analysis of the Parameter Errors and Correlations*, *Comput. Phys. Commun.* **10** (1975) 343.
- [58] J. Pumplin, D.R. Stump and W.K. Tung, *Multivariate fitting and the error matrix in global analysis of data*, *Phys. Rev. D* **65** (2001) 014011 [[hep-ph/0008191](#)].
- [59] ALEPH collaboration, *Inclusive production of pi0, eta, eta-prime (958), K0(S) and lambda in two jet and three jet events from hadronic Z decays*, *Eur. Phys. J. C* **16** (2000) 613.
- [60] S. Goyal, S.-O. Moch, V. Pathak, N. Rana and V. Ravindran, *NNLO QCD corrections to semi-inclusive DIS*, [2312.17711](#).
- [61] L. Bonino, T. Gehrmann and G. Stagnitto, *Semi-inclusive deep-inelastic scattering at NNLO in QCD*, [2401.16281](#).
- [62] J. Alwall, R. Frederix, S. Frixione, V. Hirschi, F. Maltoni, O. Mattelaer et al., *The automated computation of tree-level and next-to-leading order differential cross sections, and their matching to parton shower simulations*, *JHEP* **07** (2014) 079 [[1405.0301](#)].
- [63] R. Frederix, S. Frixione, V. Hirschi, D. Pagani, H.S. Shao and M. Zaro, *The automation of next-to-leading order electroweak calculations*, *JHEP* **07** (2018) 185 [[1804.10017](#)].

- [64] L3 collaboration, *Measurement of eta production in two and three jet events from hadronic Z decays at LEP*, *Phys. Lett. B* **371** (1996) 126.